### **Research Article**

Humaira Yasmin\*, Laila A. AL-Essa, Ali M. Mahnashi, Waleed Hamali, and Anwar Saeed\*

# A magnetohydrodynamic flow of a water-based hybrid nanofluid past a convectively heated rotating disk surface: A passive control of nanoparticles

https://doi.org/10.1515/rams-2024-0054 received April 23, 2024; accepted August 13, 2024

**Abstract:** One of the basic fluid mechanics problems of fluid flows over a revolving disk has both theoretical and real-world applications. The flow over a rotating disk has been the subject of numerous theoretical studies because it has many real-world applications in areas like rotating machinery, medical equipment, electronic devices, and computer storage. It is also crucial for engineering processes. Therefore, this article deals with a time-independent waterbased hybrid nanofluid flow containing copper oxide and silver nanoparticles past a spinning disk. The Newtonian flow is taken into consideration in this analysis. The influence of magnetic field, thermophoresis, nonlinear thermal radiation, Brownian motion, and activation energy has been considered. The present analysis is modeled in a partial differential equation form and is then converted to ordinary differential equations using appropriate variables. A numerical solution using the bvp4c technique is accomplished using MATLAB software. The current results are matched with the previous literature and established a close relationship with previous studies. The purpose of this investigation is to numerically investigate the time-independent hybrid nanofluid flow comprising copper oxide and silver nanoparticles over a rotating disk surface. The results show that the increased magnetic parameters increase the friction force at the surface, which decreases the radial and azimuthal velocity distribution. At the sheet surface, the radial velocity of the hybrid nanofluid shows dominant performance compared to the nanofluid. On the other hand, the magnetic factor has dominant behavior on the azimuthal velocity component of the nanofluid flow compared to the hybrid nanofluid flow. The higher volume fraction and magnetic factor enhance the skin friction at the disk surface. Furthermore, greater surface drag is found for the hybrid nanofluid flow. The higher solid volume fraction, temperature ratio, and Biot number enhance the rate of heat transmission. Also, a higher rate of heat transmission is observed for the hybrid nanofluid flow.

**Keywords:** MHD, hybrid nanofluid, nonlinear thermal radiation, activation energy, heat source

### **Nomenclature**

$r, \psi, z$	coordinate system
<i>u</i> , <i>w</i> , <i>v</i>	velocity components
$\Omega$	angular velocity
$B_0$	strength of the magnetic field
$T_{\rm f}$ , $T_{\rm w}$ , $T_{\infty}$	reference, surface, and ambient temperatures
$C_{\rm f}$ , $C_{\rm w}$ , $C_{\infty}$	reference, surface, and ambient
	concentrations
δ	exponential index
p	pressure
μ	dynamic viscosity
σ, <i>k</i>	electrical and thermal conductivities
$\mathcal{C}_{\mathrm{p}}$	specific heat
Q	coefficient of heat source
ν	kinematic viscosity
$D_{ m T}$	thermophoretic coefficient

Brownian diffusion coefficient

**Ali M. Mahnashi, Waleed Hamali:** Department of Mathematics, College of Science, Jazan University, Jazan, Saudi Arabia

 $D_{\rm B}$ 

<sup>\*</sup> Corresponding author: Humaira Yasmin, Department of Basic Sciences, General Administration of Preparatory Year, King Faisal University, P.O. Box 400, Al Ahsa, 31982, Saudi Arabia; Department of Mathematics and Statistics, College of Science, King Faisal University, P.O. Box 400, Al Ahsa, 31982, Saudi Arabia, e-mail: hhassain@kfu.edu.sa

<sup>\*</sup> Corresponding author: Anwar Saeed, Department of Mathematics, Abdul Wali Khan University, Mardan, 23200, Khyber Pakhtunkhwa, Pakistan, e-mail: anwarsaeed769@gmail.com

**Laila A. AL-Essa:** Department of Mathematical Sciences, College of Science, Princess Nourah bint Abdulrahman University, P.O. Box 84428, Riyadh, 11671, Saudi Arabia

2 — Humaira Yasmin et al. DE GRUYTER

$k_{ m r}$	chemical reaction coefficient
M	magnetic factor
Pr	Prandtl number
ω	temperature difference factor
$Q_{\mathrm{e}}$	exponential heat source factor
Bi	thermal Biot number
Rd	radiation factor
Nt	thermophoresis factor
Nb	Brownian motion factor
Sc	Schmidt number
Ε	activation energy factor
$K_{\rm r}$	chemical reaction factor
$ heta_{ m w}$	temperature ratio factor
$F(\eta)$	radial velocity component
$G(\eta)$	azimuthal velocity component

# **Subscripts**

f, nf, hnf base fluid, nanofluid, and hybrid nanofluid

 $egin{array}{ll} s_1 & ext{CuO nanoparticle} \\ s_2 & ext{Ag nanoparticle} \\ \end{array}$ 

### 1 Introduction

In the past, the cooling of various devices in industry and different engineering applications was challenging. Pure fluids like water and engine oil have lower thermal flow characteristics. Therefore, there was a need to enhance such flow characteristics of pure fluids. Scientists and researchers have performed various experiments to attain this goal and have modeled various approaches in this regard. The mixture of tiny-sized particles with pure fluid is one such approach, as introduced by Choi and Eastman [1]. Afterward, a new door opened in the literature to enhance the thermal characteristics of pure fluids in a variety of ways. Shahzad et al. [2] examined the convergence of second order for EMHD nanofluid on a rotating disk with the Hall effect and concluded that the volume fraction has a tremendous impact on fluid motion and heat transportation. Shamshuddin et al. [3] deliberated on dissipative and radiation mechanisms for nanofluid flow upon a disk where the flow was encountered by the Hall current. Pasha et al. [4] investigated statistically the viscous nanofluid flow on an elongating sheet and uncovered that fluid velocity deteriorated and heat flow improved for growth at nanoparticle concentration. Shah et al. [5] used nanoparticles of gold in blood to optimize its thermal flow

characteristics subject to thermally radiative effects between two plates. Asghar and Ying [6] studied 2-D radiative and mixed convective nanofluid flow on an exponentially contracting surface with impacts of partial slip constraints and observed that an upsurge in radiation factor supported the growth in thermal characteristics. Khan et al. [7] debated the nanofluid flow on a heated moving needle using chemically reactive and viscous dissipative effects. Haider et al. [8] discussed computationally a comparative work for a bloodmathematical model with impacts of magnetic field and nanoparticles. Akhtar et al. [9] carried out a dynamical analysis with computational evaluation for endoscopy of the left artery and simulated that flow arriving at the slender section of stenosis attained a maximum velocity. Naveed Khan et al. [10] studied stagnant point flow for the nanofluid of second grade on an exponentially elongating surface and established that thermal distribution augmented for higher Brownian and thermophoresis factors. Ahsan et al. [11] discussed bio-convective Darcy flow on a curved elongating surface with impacts of heterogeneous and homogenous reactions and observed that the velocity of fluid declined with growth in magnetic and porosity factors. Kanwal et al. [12] studied the dynamics of nanofluid flow with nonlinear and linear mixed convective thermal radiations and activated energy on a gyrating disk.

Recently, it has been proved that the thermal conductivities of pure fluid can be upgraded more by collaborating two types of nanoparticles in these fluids, which are known as hybrid nanofluids. Waseem et al. [13] scrutinized the mixed convective flow of hybrid nanofluid with the combined impression of the magnetic field, homogenous and heterogeneous reactions. Hussain et al. [14] used a sintered copper wick pipe to discuss experimentally the thermal performance of hybrid nanoparticles. Guedri et al. [15] discussed nanofluid flow over a nonlinear stretched sheet using various effects of the flow of the fluid. Zhang et al. [16] examined the magnetohydrodynamics (MHD) nanofluid flow on an elastic surface by mixing nanoparticles of tantalum and nickel and proved that the velocity of fluid increased with growth in tantalum nanoparticles and Darcy number while magnetic effects opposed the fluid motion. Ojjela [17] investigated numerically the heat transference of nanofluid and depicted that the thermal transportation rate increased with alumina nanoparticles compared with silica nanoparticles. Gumber et al. [18] debated the thermal characteristics of the hybrid nanoparticles past a plate and concluded that the growth in suction had a positive impact on the fluid velocity. Sriharan et al. [19] used the hybrid nanofluid flow through a tube subject to the heat source and concluded that the Nusselt number improved by 28.4% for the Al<sub>2</sub>O<sub>3</sub>/CuO-DIW hybrid nanofluid. Ullah et al. [20] examined thermal and mass flow characteristics for magnetized nanofluid flow on a cone with convective conditions at the boundary. Zawawi et al. [21] used a hybrid nano-lubricant flow with different composition ratios of nanoparticles to augment the thermal behavior of the air-conditioned system. Asghar et al. [22] inspected magnetized 3-D gyratory nanofluid flow on contracting and expanding surfaces and noticed that thermal panels augmented with growth in Eckert number and radiation factor. Babar et al. [23] inspected the effectiveness of H<sub>2</sub>Obased ferric oxide-silica hybrid nanofluid flow to investigate the airfoil-designed pin-fin with a heat sink. They deduced that the Nusselt number enhanced with a thermal power of 75 W. Akbar et al. [24] studied magnetized thermal transportation for a dual-phase nanofluid flow model using the impacts of thermal radiations and ANN approach for the solution and noticed that thermal flow augmented with an increase in the radiation factor. Ullah et al. [25] evaluated analytically the 3-D problem of a condensed film on a gyrating disk. Raja et al. [26] studied nanofluid flow on a gyratory disk with impacts of particle slip and magnetic field effects and matched the efficiency of their designed LMB-NN methodology through a comparative study and performance by utilizing error histograms, regression, and correlation. Ullah et al. [27] discussed computationally the magnetized squeezed flow for the Jeffery fluid in a gyrating frame with the mass and heat flux model suggested by Cattaneo-Christov.

MHD, a discipline at the intersection of fluid dynamics and electromagnetism, investigates the intricate interplay between magnetic fields and electrically conductive fluids [28]. In the specific perspective of heat transfer for fluid flow on a disk, MHD manifests profound impacts on the thermal behavior. As a magnetic field permeates the electrically conductive fluid, it induces electric currents, creating a dynamic coupling between the magnetic field and the fluid motion. This interaction significantly alters the flow patterns around the disk, influencing the velocity profiles and modifying the thickness of the boundary layer. MHD normally enhances heat transfer, contingent upon factors such as the orientation and strength of the magnetic field, as well as fluid properties [29,30]. In instances where MHD promotes enhanced heat transfer, it does so by fostering better mixing and circulation of the fluid near the disk's surface [31]. Additionally, the magnetic Reynolds number, indicative of the dominance of magnetic effects, plays a crucial role in determining the overall impact on heat transfer. The complex relationship of these factors is further compounded by the potential development of instabilities and turbulence within the fluid flow induced by MHD, thereby influencing the stability and proficiency of heat transfer phenomena [32]. Solving the complex system of coupled fluid flow problem, heat transfer, and electromagnetic fields is fundamental in comprehending the multifaceted implications of MHD on

heat transfer. Asghar *et al.* [33] evaluated double solutions for rotary convective 3-D nanofluid flow on contracting and expanding surfaces. Rasool *et al.* [34] examined time-based double solutions for hybrid nanofluid flow subject to slip and magnetic constraints and found that flow is retarded in the first solution with an increase in nanoparticles' volumetric fraction of copper. Lund *et al.* [35] discussed Casson magnetized nanofluid flow on a moveable and permeable surface subject to Joule heating and thermally radiative effects.

Nonlinear thermal radiation is the process of heat transfer through electromagnetic waves emitted by a surface that displays a non-linear association between the temperature and radiative heat flux. In traditional linear thermal radiation, the Stefan-Boltzmann law is employed to describe the radiant heat exchange, assuming a linear proportionality between the temperature and emitted radiation. However, in nonlinear thermal radiation, the radiative properties of the material, such as emissivity and absorptivity, are temperature-dependent in a non-linear manner [36]. This nonlinearity introduces complexities in predicting and analyzing heat transfer phenomena. The impacts of nonlinear thermal radiation on heat transfer are profound, influencing several key aspects. First, it alters the radiative heat transfer rates between surfaces, deviating from the simpler linear relationships. This can lead to significant variations in temperature distributions and thermal gradients within a system. Second, nonlinear thermal radiation complicates the design and optimization of heat exchange systems, as traditional linear models may not accurately capture the intricate temperature-dependent radiative properties of the materials. In applications such as high-temperature processes, combustion, or space exploration, where radiative heat transfer plays a critical role, accounting for nonlinear thermal radiation becomes essential for precise and reliable thermal analysis [37]. Additionally, in scenarios involving materials with temperature-sensitive optical properties, nonlinearity can impact the overall energy balance and thermal performance of the system. Accurate modeling of nonlinear thermal radiation is crucial for advancing technologies in fields, such as aerospace, materials science, and energy systems, where a nuanced understanding of heat transfer phenomena is vital for optimizing efficiency, durability, and safety. Shaw et al. [38] examined the features of linear and nonlinear radiations on MHD liquid flow on a cylinder and scrutinized the thermal flow characteristics using the values of Prandtl number in the range  $10^{-10} \le Pr \le 10^4$ .

An exponential heat source denotes a heat generation term in the energy equation, which is proportional to an exponential function of temperature. The exponential nature of the heat source implies that as the temperature increases, the heat generation rate diminishes exponentially [39]. The impact of an exponential heat source on the heat transfer phenomena is significant, introducing nonlinearity and influencing temperature distributions within a system [40]. As the temperature increases, the heat generation decreases rapidly, potentially leading to complex spatial and temporal variations in the temperature field [41]. The impact of an exponential heat source is crucial in applications like electronics cooling, combustion processes, and materials processing, where accurate prediction of temperature profiles is essential for optimizing efficiency, preventing overheating, and ensuring the integrity of the system [42]. Modeling of exponential heat sources in heat transfer simulations is imperative for designing and engineering systems that effectively manage thermal loads and maintain desired temperature conditions in diverse technological contexts [43]. Haq et al. [44] explored the impact of exponential heating sources on second-grade MHD fluid flow subject to chemically reactive effects.

A lower quantity of energy, mandatory to start a reaction chemically, is called activation energy. Algarni et al. [45] inspected the motivation of activated energy on a Casson fluid flow over a spinning disk. Rekha et al. [46] debated the activation energy influence on the motion of nanoparticles through wedge, cone, and plate and deduced that mass transportation augmented more slowly for the flow of fluid past a cone in comparison to flow on a wedge or plate. Abbasi et al. [47] scrutinized the fluid flow at the stagnant point of a horizontal cylinder subject to activation energy and perceived that with augmentation in the chemical reaction and temperature gradient factors, the mass diffusion declined. Ayub et al. [48] investigated the activation energy impact upon nanofluid flow on a cylindrical surface using inclined magnetic effects and deduced that an increase in the magnetic factor amplified the energy and weakened the velocity of the fluid flow (Table 1).

One of the basic fluid mechanics problems of fluid flows over a revolving disk has both theoretical and real-world applications. The flow on a gyrating disk has remained the subject of numerous theoretical studies because it has many real-world applications in areas like rotating machinery, medical equipment, electronic devices, and computer storage.

**Table 1:** Thermophysical features of the water nanofluid, copper oxide, and silver nanoparticles [55]

Base fluid and nanoparticles	H <sub>2</sub> O	CuO	Ag
$\sigma \left[\Omega \cdot m^{-1}\right]$	0.05	$2.70 \times 10^{-8}$	6.30 × 10 <sup>7</sup>
$k \text{ [W·m}^{-1} \cdot \text{K}^{-1}]$	0.613	76.5	429
$C_{\rm p}$ [J·kg <sup>-1</sup> ·K <sup>-1</sup> ] $\rho$ [kg·m <sup>-3</sup> ]	4,179	531.8	235
$\rho$ [kg·m <sup>-3</sup> ]	997.1	6,320	10,500
Pr	6.2	_	_

It is also crucial to engineering processes. In this attempt, we have considered the time-independent hybrid nanofluid flow over a rotating disk. Newtonian flow is taken into consideration in this analysis. The fluid flow is influenced by the magnetic field, exponential heat source, Brownian motion, chemical reaction, activation energy, thermophoresis, and nonlinear thermal radiation. By incorporating a number of complex phenomena into the modeling of hybrid nanofluid flow, this work improves the field and provides a more comprehensive knowledge of the dynamics at play. Nonlinear thermal radiation and exponential heat sources are included, which is a major improvement over earlier models that frequently omitted these features. We obtain high precision in our numerical solutions using the bvp4c technique to solve the ordinary differential equations (ODEs). This provides a solid foundation for further research into similar systems. The thorough validation procedure guarantees the validity of our results, significantly advancing the current state of fluid dynamics and heat transfer research. A mathematical model is presented in the partial differential equation form and is converted to ODEs using appropriate transformations in Section 2. The numerical solution of the existing model is obtained using the bvp4c technique in Section 3. The model validation is done in Section 4. The results of embedded factors on velocity profiles and detailed discussion are provided in Section 5, while the closing comments are listed in Section 6.

# 2 Formulation of the problem

Assume a time-independent water-based hybrid nanofluid containing copper oxide and silver nanoparticles on a gyrating disk with angular velocity  $\Omega$  along the z-direction. The cylindrical coordinates system  $(r, \psi, z)$  along the u-,v-, and w-directions is chosen for the existing problem. In the normal direction of the fluid flow, a magnetic field of strength  $B_0$  is employed. The fluid, surface, and ambient temperatures and concentrations are  $T_f$ .  $C_f$ .  $T_w$ ,  $C_w$ ,  $T_\infty$ , and  $C_\infty$  such that  $T_f > T_w$ ,  $C_f > C_w$ . A geometrical representation is displayed in Figure 1. Additionally, to understand the flow behavior, the following suppositions are made in this investigation:

- The flow is Newtonian.
- Impacts of the Hall current and induced magnetic field have been ignored.
- The significance of nonlinear linear thermal radiation, Brownian motion, and thermophoresis are accounted for.
- The flow is impacted by the chemical reaction with activation energy.

Thus, the main equations are defined as follows [49–51]:

$$u = 0, \ v = r\Omega, \ w = 0, \ -k_{mf} \frac{\partial T}{\partial z} = h_f \left(T - T_f\right), \ D_B \frac{\partial C}{\partial z} + \frac{D_T}{T_\infty} \frac{\partial T}{\partial z} = 0$$
Surface conditions

Figure 1: Geometry of flow problem.

$$\frac{\partial u}{\partial r} + \frac{\partial w}{\partial z} + \frac{u}{r} = 0, \tag{1}$$

$$u\frac{\partial u}{\partial r} - \frac{v^2}{r} + w\frac{\partial u}{\partial z} = -\frac{1}{\rho_{\rm hnf}} \frac{\partial p}{\partial r} + \frac{\mu_{\rm hnf}}{\rho_{\rm hnf}} \left[ \frac{\partial^2 u}{\partial r^2} + \frac{1}{r} \frac{\partial u}{\partial r} - \frac{u}{r} + \frac{u}{\rho_{\rm hnf}} \frac{\partial v}{\partial r} + \frac{u}{r} \frac{\partial v}{\partial r} \right] \tag{2}$$

$$-\frac{u}{r^2} + \frac{\partial^2 u}{\partial z^2} - \frac{\sigma_{\rm hnf}}{\rho_{\rm hnf}} B_0^2 u, \tag{2}$$

$$u\frac{\partial v}{\partial r} + w\frac{\partial v}{\partial z} + \frac{uv}{r} = \frac{\mu_{\rm hnf}}{\rho_{\rm hnf}} \left[ \frac{\partial^2 v}{\partial r^2} - \frac{v}{r^2} + \frac{1}{r} \frac{\partial v}{\partial r} + \frac{\partial^2 v}{\partial z^2} \right] - \frac{\sigma_{\rm hnf}}{\rho_{\rm hnf}} B_0^2 v, \tag{3}$$

$$w\frac{\partial w}{\partial z} + u\frac{\partial w}{\partial r} = -\frac{1}{\rho_{\rm hnf}} \frac{\partial p}{\partial z} + \frac{\mu_{\rm hnf}}{\rho_{\rm hnf}} \left[ \frac{\partial^2 w}{\partial r^2} + \frac{\partial^2 w}{\partial z^2} + \frac{1}{r} \frac{\partial w}{\partial r} \right] + \frac{1}{(\rho C_p)_{\rm hnf}} \left[ \frac{\partial \sigma^2 v}{\partial r^2} + \frac{1}{r} \frac{\partial v}{\partial r} + \frac{\partial \sigma^2 v}{\partial z^2} \right] + \frac{1}{(\rho C_p)_{\rm hnf}} \left[ \frac{\partial \sigma^2 v}{\partial r^2} + \frac{1}{r} \frac{\partial v}{\partial r} + \frac{\partial \sigma^2 v}{\partial z} \right] + \frac{\rho v}{(\rho C_p)_{\rm hnf}} \left[ \frac{\partial \sigma^2 v}{\partial r} + \frac{\partial \sigma^2 v}{\partial z} + \frac{\partial \sigma^2 v}{\partial z} \right] + \frac{\rho v}{T_{\infty}} \left[ \left( \frac{\partial \sigma}{\partial r} \right)^2 + \left( \frac{\partial \sigma}{\partial z} \right)^2 \right] + \frac{\rho v}{T_{\infty}} \left[ \left( \frac{\partial \sigma}{\partial r} \right)^2 + \left( \frac{\partial \sigma}{\partial z} \right)^2 \right] + \frac{\rho v}{T_{\infty}} \left[ \frac{\partial \sigma}{\partial r} \right] + \frac{\rho v}{T_$$

The constraints at the boundary are [52]

$$\begin{cases} u = 0, w = 0, v = \Omega r, -k_{\rm hnf} \frac{\partial T}{\partial z} = h_{\rm f}(T_{\rm f} - T), \\ \frac{D_T}{T_{\infty}} \frac{\partial T}{\partial z} + D_{\rm B} \frac{\partial C}{\partial z} = 0 \text{ at } z = 0, \\ u \to 0, T \to T_{\infty}, v \to 0, C \to C_{\infty} \text{ as } z \to \infty \end{cases}$$
 (7)

The thermophysical features of the nanofluid/hybrid nanoparticles are expressed as follows [52–54]:

$$\begin{cases} \mu = \frac{1}{(1-\chi)^{2.5}}, (\rho C_{\rm p})_{\rm nf} = (\rho C_{\rm p})_{\rm f} (1-\chi) + \chi (\rho C_{\rm p})_{\rm s}, \\ \rho_{\rm nf} = \chi \rho_{\rm s} + \rho_{\rm f} (1-\chi), \\ \sigma_{\rm nf} = \left[ \frac{\sigma_{\rm s} + 2 \sigma_{\rm f} - 2(\sigma_{\rm f} - \sigma_{\rm s})\chi}{\sigma_{\rm s} + 2 \sigma_{\rm f} + (\sigma_{\rm f} - \sigma_{\rm s})\chi} \right] \sigma_{\rm f}, \\ k_{\rm nf} = \left[ \frac{k_{\rm s} - 2(k_{\rm f} - k_{\rm s})\chi + 2k_{\rm f}}{k_{\rm s} + (k_{\rm f} - k_{\rm s})\chi + 2k_{\rm f}} \right] k_{\rm f}, \end{cases}$$
(8)

$$k_{\text{hnf}} = \begin{bmatrix} \frac{\chi_{1}k_{s_{1}} + \chi_{2}k_{s_{2}}}{(\chi_{2} + \chi_{1})} + 2k_{f} + 2(\chi_{1}k_{s_{1}} + \chi_{2}k_{s_{2}}) - 2k_{f}(\chi_{2} + \chi_{1}) \\ \frac{\chi_{1}k_{s_{1}} + \chi_{2}k_{s_{2}}}{(\chi_{2} + \chi_{1})} + 2k_{f} - 2(\chi_{1}k_{s_{1}} + \chi_{2}k_{s_{2}}) + k_{f}(\chi_{2} + \chi_{1}) \end{bmatrix} k_{f},$$

$$\rho_{\text{hnf}} = (1 - \chi_{1} - \chi_{2})\rho_{f} + \chi_{1}\rho_{s_{1}} + \chi_{2}\rho_{s_{2}}, \mu_{\text{hnf}} = \frac{\mu_{f}}{(1 - \chi_{1} - \chi_{2})^{2.5}},$$

$$(\rho C_{p})_{\text{hnf}} = (1 - \chi_{1} - \chi_{2})(\rho C_{p})_{f} + (\rho C_{p})_{2}\rho_{s_{2}} + \chi_{1}(\rho C_{p})_{s_{1}},$$

$$\sigma_{\text{hnf}} = \begin{bmatrix} \frac{\chi_{1}\sigma_{s_{1}} + \chi_{2}\sigma_{s_{2}}}{(\chi_{2} + \chi_{1})} + 2\sigma_{f} + 2(\sigma_{s_{1}}\chi_{1} + \sigma_{s_{2}}\chi_{2}) - 2\sigma_{f}(\chi_{2} + \chi_{1}) \\ \frac{\chi_{1}\sigma_{s_{1}} + \chi_{2}\sigma_{s_{2}}}{(\chi_{2} + \chi_{1})} + 2\sigma_{f} - 2(\sigma_{s_{1}}\chi_{1} + \sigma_{s_{2}}\chi_{2}) + \sigma_{f}(\chi_{2} + \chi_{1}) \end{bmatrix} \sigma_{f}.$$

$$(9)$$

A set of appropriate [49,56,57]:

$$u = r\Omega F(\eta), v = r\Omega G(\eta), w = \sqrt{\Omega \nu_{\rm f}} H(\eta),$$

$$p - p_{\infty} = 2\mu_{\rm f} \Omega p(\eta)$$

$$T = T_{\infty} (1 + (\theta_{\rm W} - 1)\theta(\eta)), \phi(\eta) = \frac{C - C_{\infty}}{C_{\infty}}, \eta = \sqrt{\frac{\Omega}{\nu_{\rm f}}} z.$$
(10)

Using Eq. (10) in Eqs. (1)–(6), we have

$$H' + 2F = 0, (11)$$

$$\left(\frac{\mu_{\rm hnf}/\mu_{\rm f}}{\rho_{\rm hnf}/\rho_{\rm f}}\right)F'' - F^2 + G^2 - HF' - \left(\frac{\sigma_{\rm hnf}/\sigma_{\rm f}}{\rho_{\rm hnf}/\rho_{\rm f}}\right)MF = 0, \quad (12)$$

$$\left(\frac{\mu_{\rm hnf}/\mu_{\rm f}}{\rho_{\rm hnf}/\rho_{\rm f}}\right)G'' - 2FG - HG' - \left(\frac{\sigma_{\rm hnf}/\sigma_{\rm f}}{\rho_{\rm hnf}/\rho_{\rm f}}\right)MG = 0, \quad (13)$$

$$\left(\frac{k_{\text{hnf}}}{k_{\text{f}}} + \text{Rd}(1 + \theta(\theta_{\text{w}} - 1))^{3}\right)\theta'' + 4\text{Rd}(\theta_{\text{w}})$$

$$-1)(1 + (\theta_{\text{w}} - 1)\theta)^{2} \theta'^{2} - \text{Pr}\frac{(\rho C_{\text{p}})_{\text{hnf}}}{(\rho C_{\text{p}})_{\text{f}}}H\theta'$$

$$+ \text{PrNt}\theta'^{2} + \text{PrNb}\theta'\phi' + Q_{e}\exp(-\delta\eta) = 0,$$
(14)

$$\phi'' + \frac{Nt}{Nb}\theta'' - ScH\phi' - KrSc(1 + \omega\theta)^n \phi \exp\left(\frac{E}{(1 + \omega\theta)}\right) = 0.$$
(15)

Transformed constraints at the boundary are as follows:

$$\begin{cases} F(0) = 0, H(0) = 0, G(0) = 1, \frac{k_{\text{hnf}}}{k_{\text{f}}} \theta'(0) \\ = -\text{Bi}(1 - \theta(0)), \phi'(0) + \left(\frac{\text{Nt}}{\text{Nb}}\right) \theta'(0) = 0, \\ F(\infty) = 0, G(\infty) = 0, \theta(\infty) = 0, \phi(\infty) = 0. \end{cases}$$
(16)

The emerging factors are as follows:

$$\begin{cases} M = \frac{\sigma_{\rm f} B_0^2}{\rho_{\rm f} \Omega}, \, \Pr = \frac{\nu_{\rm f} (\rho C_{\rm p})_f}{k_{\rm f}}, \, \omega = \frac{T_{\rm f} - T_{\infty}}{T_{\infty}}, \\ Q_{\rm e} = \frac{Q}{\Omega(\rho C_{\rm p})_f}, \, \text{Bi} = \frac{h_{\rm f}}{k_{\rm f}} \sqrt{\frac{\nu_{\rm f}}{\Omega}}, \, \text{Rd} = \frac{16\sigma^*}{3k^*} \frac{T_{\infty}^3}{k_{\rm f}}, \\ \text{Nt} = \frac{(\rho C_{\rm p})_{\rm np} D_{\rm T} (T_{\rm f} - T_{\infty})}{(\rho C_{\rm p})_{\rm f} T_{\infty} \nu_{\rm f}}, \, \text{Nb} = \frac{(\rho C_{\rm p})_{\rm np} D_{\rm B} C_{\infty}}{(\rho C_{\rm p})_{\rm f} \nu_{\rm f}}, \\ \text{Sc} = \frac{\nu_{\rm f}}{D_{\rm B}}, \, E = \frac{E_{\rm a}}{k_{\rm b} T_{\infty}}, \, K_{\rm r} = \frac{k_{\rm r}^2}{\Omega}, \, \theta_{\rm w} = \frac{T_{\rm f}}{T_{\infty}}. \end{cases}$$

$$(17)$$

$$= -\frac{\left(\Re(4))^2 - (\Re(2))^2 - \Re(1)\Re(3) - \frac{\sigma_{\rm hnf}/\sigma_{\rm f}}{\rho_{\rm hnf}/\rho_{\rm f}} \Re\Re(2)\right)}{\left(2\Re(2)\Re(4) + \Re(1)\Re(5) + \frac{\sigma_{\rm hnf}/\sigma_{\rm f}}{\rho_{\rm for}} M\Re(4)\right)}$$

The skin friction (coefficient) and Nusselt number are described mathematically as

$$C_{\text{fr}} = \frac{\sqrt{\tau_{\text{wr}}^2 + \tau_{\text{wz}}^2}}{\rho_{\text{f}}(\Omega r)^2}, \text{Nu}_{\text{r}} = \frac{rq_{\text{w}}}{k_{\text{f}}(T_{\text{f}} - T_{\infty})},$$
 (18)

$$=\frac{1}{\rho_{\rm f}(\Omega r)^2}$$
,  $Nu_{\rm r} = \frac{1}{k_{\rm f}(T_{\rm f} - T_{\infty})}$ , (16)

 $\mathfrak{R}'(7) = -\frac{\left[ \text{Rd}(\theta_{\text{W}} - 1)(1 + (\theta_{\text{W}} - 1)\mathfrak{R}(6))^{2}(\mathfrak{R}(7))^{2} - \text{Pr}\frac{(\rho C_{\text{p}})_{\text{hnf}}}{(\rho C_{\text{p}})_{\text{f}}}\mathfrak{R}(1)\mathfrak{R}(7) + \right]}{\left[ \frac{k_{\text{hnf}}}{k_{\text{f}}} + \text{Rd}(1 + (\theta_{\text{W}} - 1)\mathfrak{R}(6))^{3} \right]}$ 

where

$$\tau_{\text{WT}} = \mu_{\text{hnf}} \left( \frac{\partial u}{\partial z} + \frac{\partial w}{\partial r} \right) \Big|_{z=0}, 
\tau_{\text{WZ}} = \mu_{\text{hnf}} \left[ \left( \frac{1}{r} \right) \frac{\partial w}{\partial \psi} + \frac{\partial v}{\partial z} \right] \Big|_{z=0}.$$
(19)

Thus, the above equation is reduced to

$$\sqrt{\text{Re}_{r}} C_{f} = \sqrt{G'^{2}(0) + F'^{2}(0)},$$

$$\frac{1}{\sqrt{\text{Re}_{r}}} \text{Nu} = -\left[\frac{k_{\text{hnf}}}{k_{f}} + \text{Rd}(1 + (\theta_{\text{w}} - 1)\theta(0))^{3}\right] \theta'(0),$$
(20)

where  $\operatorname{Re}_{r}^{\frac{Qr^{2}}{V_{f}}}$  is the local Reynolds number.

# 3 Numerical solution

The byp4c procedure, coded in MATLAB software, is practical and simple to use and is capable of handling problems that are somewhat complex. For the purpose of resolving nonlinear equations, this iterative approach is used [58-60]. The present numerical technique is implemented in Eqs. (11)-(15) subject to Eq. (16). First, we convert the nonlinear equations into a first-order system as follows:

$$\begin{cases} H = \Re(1), H' = \Re'(1), \\ F = \Re(2), F' = \Re(3), F'' = \Re'(3), \\ G = \Re(4), G' = \Re(5), G'' = \Re'(5), \\ \theta = \Re(6), \theta' = \Re(7), \theta'' = \Re'(7), \\ \phi = \Re(8), \phi' = \Re(9), \phi'' = \Re'(9), \end{cases}$$
(21)

$$\mathfrak{R}'(1) = -2\mathfrak{R}(2),\tag{22}$$

(25)

$$\mathfrak{R}'(3) = -\frac{\left[ (\mathfrak{R}(4))^2 - (\mathfrak{R}(2))^2 - \mathfrak{R}(1)\mathfrak{R}(3) - \frac{\sigma_{\mathrm{hnf}}/\sigma_{\mathrm{f}}}{\rho_{\mathrm{hnf}}/\rho_{\mathrm{f}}} M\mathfrak{R}(2) \right]}{\frac{\mu_{\mathrm{hnf}}/\mu_{\mathrm{f}}}{\rho_{\mathrm{hnf}}/\rho_{\mathrm{f}}}}, \tag{23}$$

$$\Re'(5) = \frac{\left[2\Re(2)\Re(4) + \Re(1)\Re(5) + \frac{\sigma_{\text{hnf}}/\sigma_{\text{f}}}{\rho_{\text{hnf}}/\rho_{\text{f}}}M\Re(4)\right]}{\frac{\mu_{\text{hnf}}/\mu_{\text{f}}}{\rho_{\text{hnf}}/\rho_{\text{f}}}}, \quad (24)$$

$$\mathfrak{R}'(9) - \left[\frac{\mathrm{Nt}}{\mathrm{Nb}}\mathfrak{R}'(7) - Sc\mathfrak{R}(1)\mathfrak{R}(9) - K_{\Gamma}\mathrm{Sc}(1 + \omega\mathfrak{R}(6))^{n}\mathfrak{R}(8) \exp\left[-\frac{E}{(1 + \omega\mathfrak{R}(6))}\right]\right]. \tag{26}$$

with the boundary conditions

Thus, the above equation is reduced to 
$$\sqrt{\text{Re}_{r}}C_{f} = \sqrt{G'^{2}(0) + F'^{2}(0)},$$

$$\frac{1}{\sqrt{\text{Re}_{r}}}\text{Nu} = -\left(\frac{k_{\text{hnf}}}{k_{\text{f}}} + \text{Rd}(1 + (\theta_{\text{w}} - 1)\theta(0))^{3}\right)\theta'(0),$$

$$\frac{1}{\sqrt{\text{Re}_{r}}}\text{Nu} = -\left(\frac{k_{\text{hnf}}}{k_{\text{f}}} + \text{Rd}(1 + (\theta_{\text{w}} - 1)\theta(0))^{3}\right)\theta'(0),$$

$$\frac{1}{\sqrt{\text{Re}_{r}}}\text{Nu} = -\left(\frac{k_{\text{hnf}}}{k_{\text{f}}} + \text{Rd}(1 + (\theta_{\text{w}} - 1)\theta(0))^{3}\right)\theta'(0),$$

$$\frac{1}{\sqrt{\text{Re}_{r}}}\text{Nu} = -\left(\frac{k_{\text{hnf}}}{k_{\text{f}}} + \text{Rd}(1 + (\theta_{\text{w}} - 1)\theta(0))^{3}\right)\theta'(0),$$

$$\frac{1}{\sqrt{\text{Re}_{r}}}\text{Nu} = -\left(\frac{k_{\text{hnf}}}{k_{\text{f}}} + \text{Rd}(1 + (\theta_{\text{w}} - 1)\theta(0))^{3}\right)\theta'(0),$$

$$\frac{1}{\sqrt{\text{Re}_{r}}}\text{Nu} = -\left(\frac{k_{\text{hnf}}}{k_{\text{f}}} + \text{Rd}(1 + (\theta_{\text{w}} - 1)\theta(0))^{3}\right)\theta'(0),$$

$$\frac{1}{\sqrt{\text{Re}_{r}}}\text{Nu} = -\left(\frac{k_{\text{hnf}}}{k_{\text{f}}} + \text{Rd}(1 + (\theta_{\text{w}} - 1)\theta(0))^{3}\right)\theta'(0),$$

$$\frac{1}{\sqrt{\text{Re}_{r}}}\text{Nu} = -\left(\frac{k_{\text{hnf}}}{k_{\text{f}}} + \text{Rd}(1 + (\theta_{\text{w}} - 1)\theta(0))^{3}\right)\theta'(0),$$

$$\frac{1}{\sqrt{\text{Re}_{r}}}\text{Nu} = -\left(\frac{k_{\text{hnf}}}{k_{\text{f}}} + \text{Rd}(1 + (\theta_{\text{w}} - 1)\theta(0))^{3}\right)\theta'(0),$$

$$\frac{1}{\sqrt{\text{Re}_{r}}}\text{Nu} = -\left(\frac{k_{\text{hnf}}}{k_{\text{f}}} + \text{Rd}(1 + (\theta_{\text{w}} - 1)\theta(0))^{3}\right)\theta'(0),$$

$$\frac{1}{\sqrt{\text{Re}_{r}}}\text{Nu} = -\left(\frac{k_{\text{hnf}}}{k_{\text{f}}} + \text{Rd}(1 + (\theta_{\text{w}} - 1)\theta(0))^{3}\right)\theta'(0),$$

$$\frac{1}{\sqrt{\text{Re}_{r}}}\text{Nu} = -\left(\frac{k_{\text{hnf}}}{k_{\text{f}}} + \text{Rd}(1 + (\theta_{\text{w}} - 1)\theta(0))^{3}\right)\theta'(0),$$

$$\frac{1}{\sqrt{\text{Re}_{r}}}\text{Nu} = -\left(\frac{k_{\text{hnf}}}{k_{\text{f}}} + \text{Rd}(1 + (\theta_{\text{w}} - 1)\theta(0))^{3}\right)\theta'(0),$$

$$\frac{1}{\sqrt{\text{Re}_{r}}}\text{Nu} = -\left(\frac{k_{\text{hnf}}}{k_{\text{f}}} + \text{Rd}(1 + (\theta_{\text{w}} - 1)\theta(0))^{3}\right)\theta'(0),$$

$$\frac{1}{\sqrt{\text{Re}_{r}}}\text{Nu} = -\left(\frac{k_{\text{hnf}}}{k_{\text{f}}} + \text{Rd}(1 + (\theta_{\text{w}} - 1)\theta(0))^{3}\right)\theta'(0),$$

$$\frac{1}{\sqrt{\text{Re}_{r}}}\text{Nu} = -\left(\frac{k_{\text{hnf}}}{k_{\text{f}}} + \text{Rd}(1 + (\theta_{\text{w}} - 1)\theta(0))^{3}\right)\theta'(0),$$

$$\frac{1}{\sqrt{\text{Re}_{r}}}\text{Nu} = -\left(\frac{k_{\text{hnf}}}{k_{\text{f}}} + \text{Rd}(1 + (\theta_{\text{w}} - 1)\theta(0))^{3}\right)\theta'(0),$$

$$\frac{1}{\sqrt{\text{Re}_{r}}}\text{Nu} = -\left(\frac{k_{\text{hnf}}}{k_{\text{f}}} + \text{Rd}(1 + (\theta_{\text{w}} - 1)\theta(0))^{3}\right)\theta'(0),$$

$$\frac{1}{\sqrt{\text{Re}_{r}}}\text{Nu} = -\left(\frac{k_{\text{hnf}}}{k_{\text{f}}} + \text{Rd}(1 + (\theta_{\text{w}} - 1)\theta(0))^{3}\right)\theta'(0),$$

$$\frac{1}{\sqrt{\text{Re}_{r}}}\text{Nu} = -\left(\frac{k_{\text{hnf}}}{k_{\text{f}}} + \text{Rd}(1 + (\theta_{\text{w}} -$$

Table 2: Validation of the current data with the available results of Turkyilmazoglu [62] and Rashidi *et al.* [61] when  $\chi_1 = \chi_2 = 0.0$ 

	F(0)		
М	1	4	
Rashidi <i>et al.</i> [61]	0.309237	0.165701	
Turkyilmazoglu [62]	0.309258	0.165703	
Present results	0.309258	0.165703	

where  $\mathfrak{R}_0$  and  $\mathfrak{R}_{inf}$  are used for the initial and boundary conditions.

### Present validation

When all other factors are zero, the existing results are compared with the results of Rashidi et al. [61] and Turkyilmazoglu [62], who also published their findings. As shown in Table 2, a similar result has been found in our present exploration.

## 5 Results and discussions

### 5.1 Results

### 5.1.1 Discussion of results

This section compacts with the impacts of embedded factors on radial and azimuthal velocity, thermal, and concentration

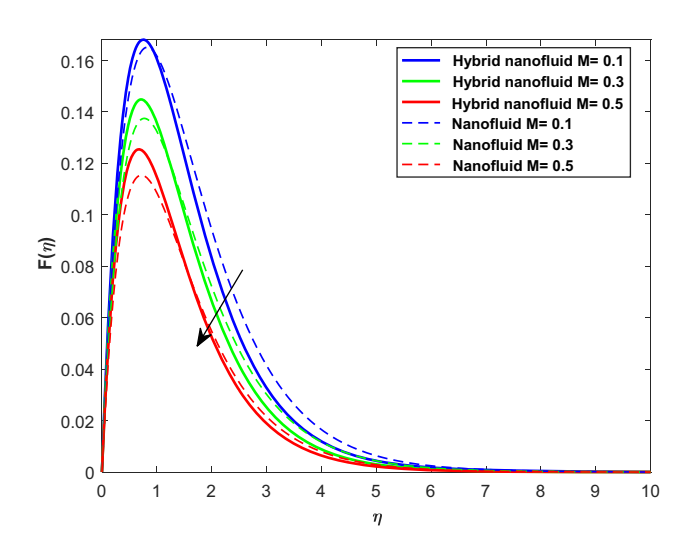


**Figure 2:** Influence of *M* on  $F(\eta)$ .

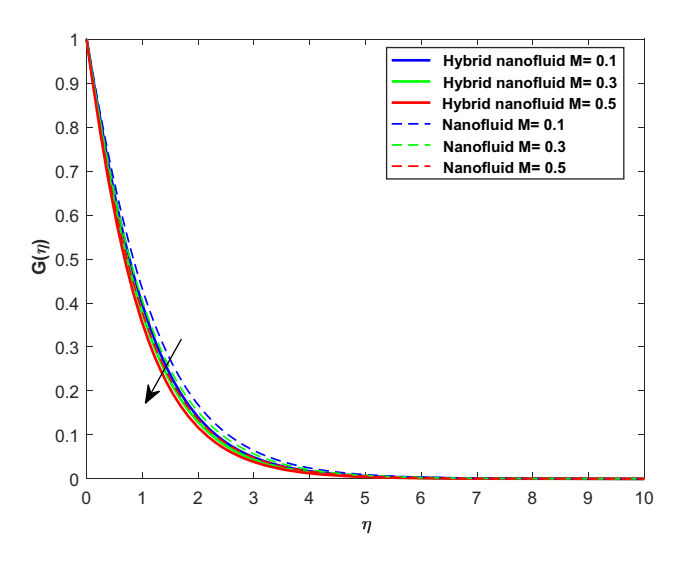


**Figure 3:** Influence of M on  $G(\eta)$ .

distributions of the fluid flow past a revolving disk. The numerical solution for the problem is evaluated using the bvp4c method. The influence of embedded factors on the flow distributions and quantities of interest is shown in Figures 2-16 and Tables 2-8. Table 2 describes a comparative analysis. Figures 2 and 3 display the influence of magnetic parameter (M) over radial velocity  $(F(\eta))$  and azimuthal velocity ( $G(\eta)$ ). From these figures, it can be observed that  $F(\eta)$ and  $G(\eta)$  reduce due to an increase of M. Actually, growth in M heightens the Lorentz force as created in the flow system, which augments the friction farce at the sheet surface and decelerates the flow. Therefore, the magnetic parameter opposes the transport phenomena, which results in the reduction of the velocity profiles, as shown in Figures 2 and 3. Hence, the velocity of the fluid in both radial and azimuthal

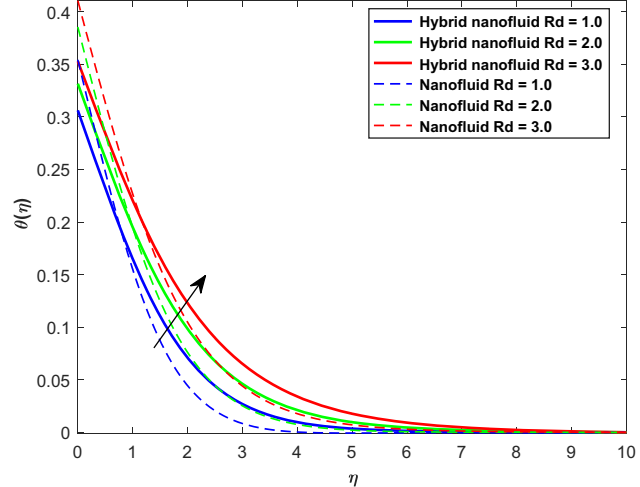


**Figure 4:** Influence of Rd on  $\theta(\eta)$ .

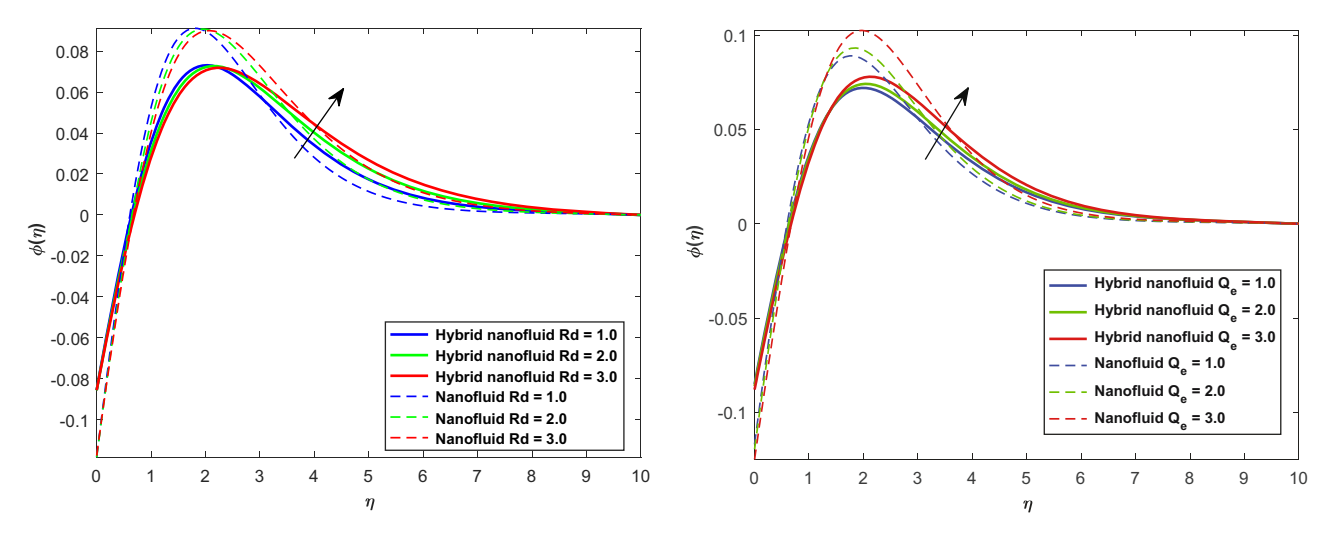


**Figure 5:** Influence of Rd on  $\phi(\eta)$ .

**Figure 8:** Influence of  $Q_{\rm e}$  on  $\phi(\eta)$ .

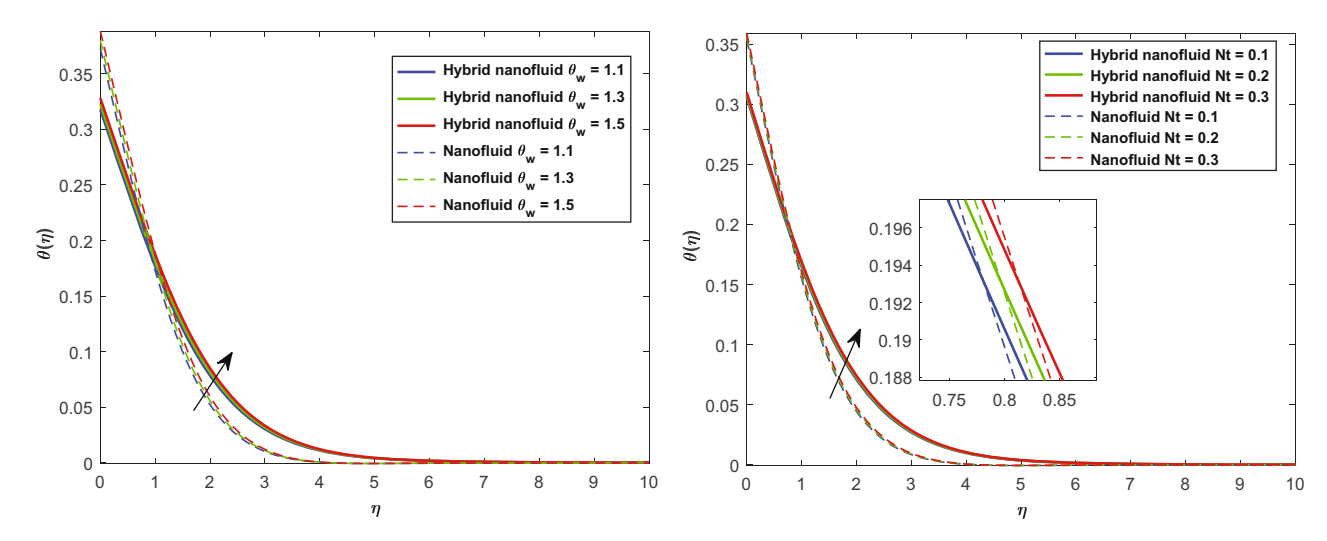


**Figure 6:** Influence of  $\theta_{w}$  on  $\theta(\eta)$ .

**Figure 9:** Influence of Nt on  $\theta(\eta)$ .

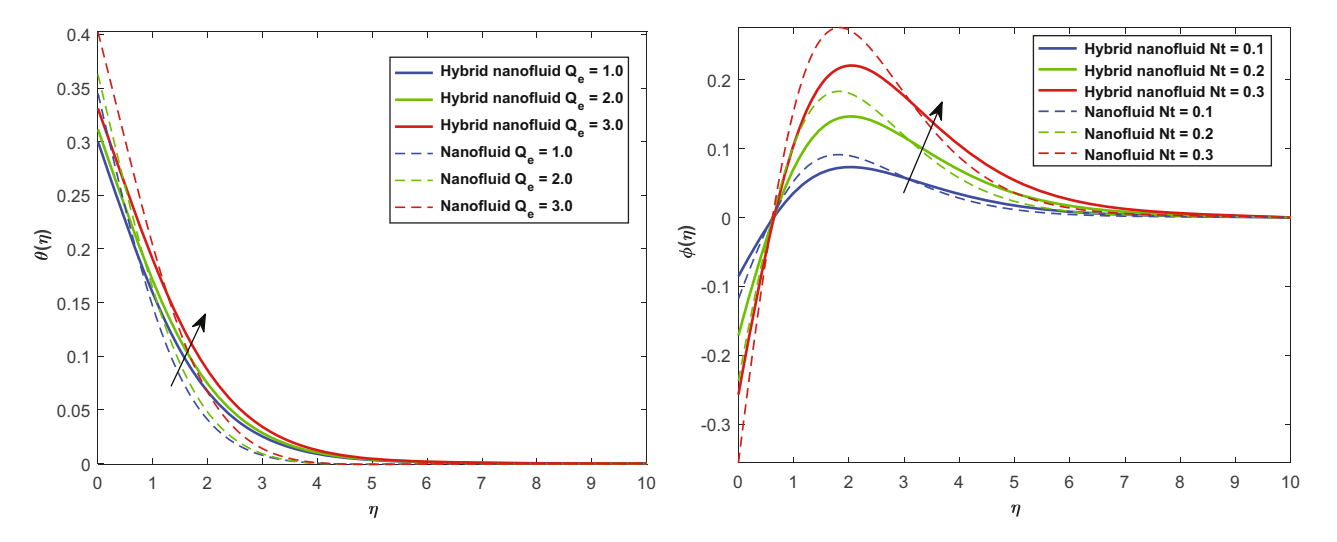
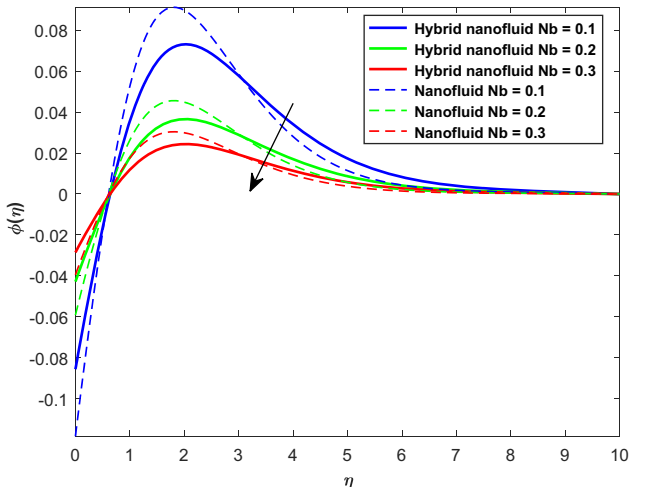


**Figure 7:** Influence of  $Q_{\rm e}$  on  $\theta(\eta)$ .

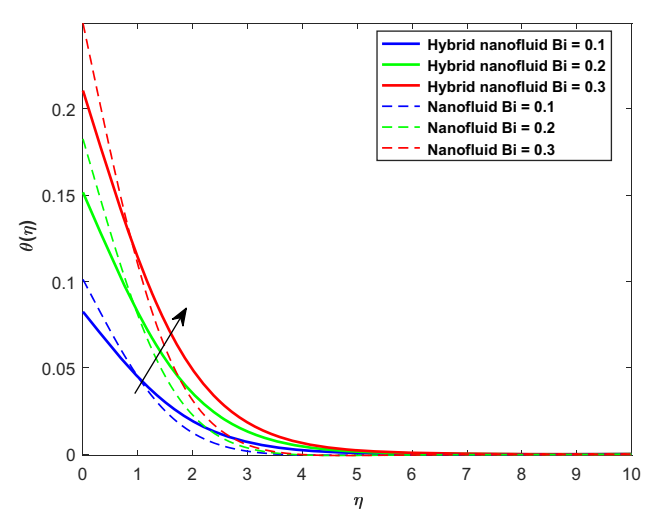
**Figure 10:** Influence of Nt on  $\phi(\eta)$ .

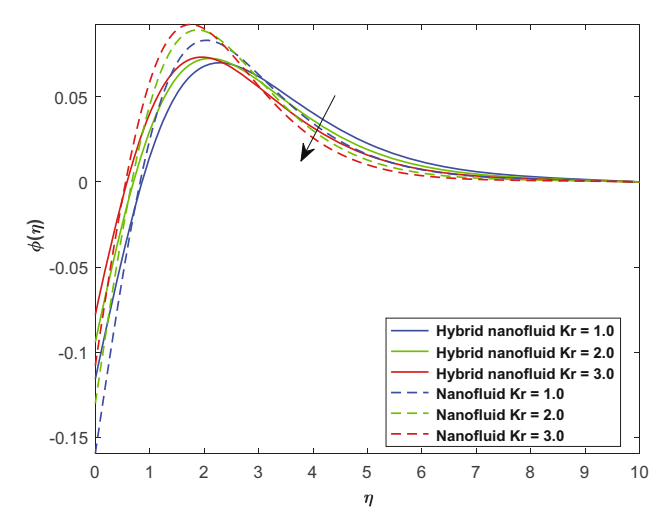


0.05 Λ Hybrid nanofluid E = 0.1 Hybrid nanofluid E = 0.2 (E) -0.05 Hybrid nanofluid E = 0.3 Nanofluid E = 0.1 Nanofluid E = 0.2 Nanofluid E = 0.3 -0 1 -0.15 0 10

**Figure 11:** Influence of Nb on  $\phi(\eta)$ .

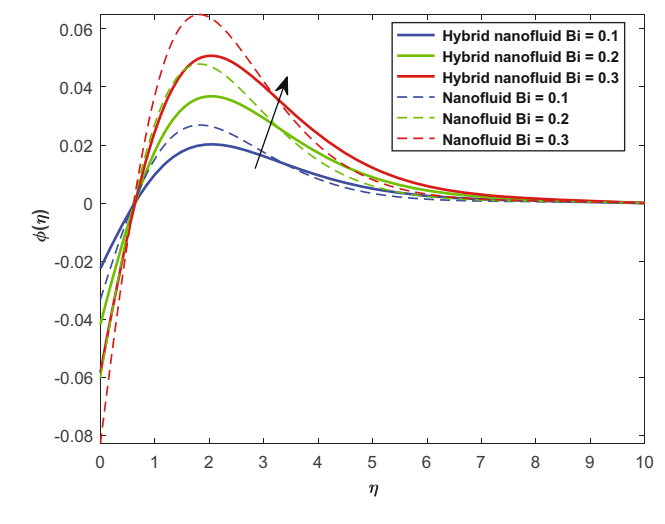
**Figure 14:** Influence of *E* on  $\phi(\eta)$ .





**Figure 12:** Influence of Bi on  $\theta(\eta)$ .

**Figure 15:** Influence of  $K_r$  on  $\phi(\eta)$ .



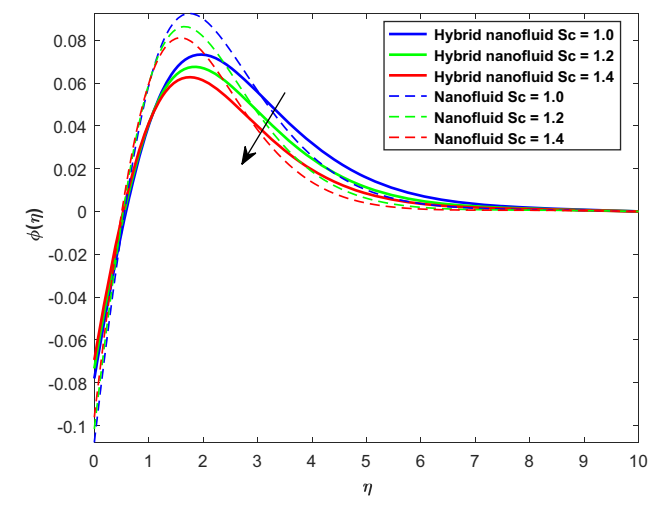


**Figure 13:** Influence of Bi on  $\phi(\eta)$ .

**Figure 16:** Influence of Sc on  $\phi(\eta)$ .

**Table 3:** Impacts of  $\chi_1$  and M on  $\sqrt{\mathrm{Re_r}} C_\mathrm{f}$ 

<b>X</b> 1	М	CuO−H₂O nanofluid
0.01	0.1	0.467647
0.02		0.476437
0.03		0.487643
0.04		0.498738
	0.3	0.397647
	0.7	0.456784
	1.3	0.549720

**Table 4:** Impacts of  $\chi_2$  and M on  $\sqrt{\text{Re}_{\rm r}} C_{\rm f}$ 

χ <sub>2</sub>	М	Ag−H₂O nanofluid
0.01	0.1	0.470863
0.02		0.480849
0.03		0.495185
0.04		0.515890
	0.3	0.415759
	0.7	0.479058
	1.3	0.568561

directions decreases due to the augmenting magnetic factor. At the sheet surface, the radial velocity of the hybrid nanofluid shows a dominant behavior compared to the nanofluid. However, this effect is reversed above the surface. Figures 4 and 5 demonstrate the impact of the radiation factor (Rd) on  $(\theta(\eta))$  and  $(\phi(\eta))$ , respectively. From these figures, it can be observed that both  $\theta(\eta)$  and  $\phi(\eta)$  reduce due to an increase of Rd. Generally, Rd is the source of external energy that provides heat to the working fluid in the electromagnetic waveform, and as a result, the temperature and concentration boundary layer thicknesses increase. Thus,  $\theta(\eta)$  and  $\phi(\eta)$ increase with an increase in the thermal radiation factor. At the sheet surface, the temperature of the nanofluid shows a dominant behavior compared to the nanofluid. However, this effect is reversed above the surface. Figure 6 shows the influence of the temperature difference factor  $\theta_{\rm w}$  on  $\theta(\eta)$ . It is

**Table 5:** Impacts of  $\chi_1$  =  $\chi_2$  and M on  $\sqrt{\mathrm{Re_r}} \, C_\mathrm{f}$ 

$\chi_1 = \chi_2$	М	CuO−Ag/H₂O hybrid nanofluid
0.01	0.1	0.588648
0.02		0.607529
0.03		0.598620
0.04		0.637863
	0.3	0.654264
	0.7	0.670834
	1.3	0.696431

**Table 6:** Impacts of  $\chi_1$ , Bi, and  $\theta_w$  on  $\frac{1}{\sqrt{Re_r}}$ Nu

<b>X</b> 1	Bi	$ heta_{\sf w}$	CuO-H <sub>2</sub> O nanofluid
0.01	0.1	1.1	0.467647
0.02			0.476437
0.03			0.487643
0.04			0.498738
	0.3		0.397647
	0.7		0.456784
	1.3		0.549720
		1.1	0.476536
		1.2	0.486525
		1.3	0.497533

noticed that the thermal distribution increases with increasing  $\theta_{\rm w}$ . The temperature difference factor shows the ratio of  $T_{\rm f}$ with  $T_{\infty}$  (i.e.,  $\theta_{\rm W} = T_{\rm f}/T_{\infty}$ ). It is also obvious that  $\theta_{\rm W}$  must be greater than 1. According to this definition, as we increase  $\theta_{w_1}$ the reference heat of fluid flow also increases, which results in a higher thermal distribution of the fluid flow. Thus, an increase in  $\theta_w$  increases  $\theta(\eta)$ . At the surface of the sheet, the temperature of the nanofluid shows a dominant behavior compared to the hybrid nanofluid. However, this effect is reversed above the surface. Figure 7 shows the impact of the heat source factor  $(Q_e)$  on  $\theta(\eta)$ . It is noticed that  $\theta(\eta)$ increases with increasing  $Q_e$ . Actually,  $Q_e$  plays an imperative role in the form of extra heat to the flow system. Because of the fundamental principles of thermodynamics, adding a heat source to a system improves its thermal profile. According to the law of conservation of energy, energy cannot be generated or destroyed, but rather transferred or changed from one form to another. As a result, the heat source provides thermal energy to the system, causing a temperature increase throughout its geographical extent. This thermal energy transfer occurs when heat naturally flows from higher temperatures (the heat source) to lower temperatures (the surroundings or the system itself), resulting in a detectable increase in the temperature throughout the system. Thus, the thermal profile reflects how the new heat is redistributed and changes the system's thermal state. Thus, an increase in  $Q_{\mathrm{e}}$  increases heta $(\eta)$ . Similarly,  $\phi(\eta)$  also increases with an increase in  $Q_{\rm e}$  as displayed in Figure 8. At the sheet surface, the temperature of the nanofluid shows a dominant behavior compared to the hybrid nanofluid. However, this effect is reversed above the surface. Figures 9 and 10 show the influence of Nt on  $\theta(\eta)$ and  $\phi(\eta)$ . It is observed that both  $\theta(\eta)$  and  $\phi(\eta)$  increase with increasing Nt. This occurs because the particles near the heated surfaces generate a thermophoretic force that pushes the particles to break down away from the fluid regime, increasing the thicknesses of concentration and temperature boundary layers. At the sheet surface, the temperature and

concentration of the nanofluid show a dominant behavior compared to the hybrid nanofluid. However, this consequence is reversed above the surface. Figure 11 shows the impact of the Brownian factor (Nb) on  $\phi(\eta)$ . It is found that an increase of Nb reduces  $\phi(\eta)$ . As Nb values increase, the concentration profile decreases, in turn the concentration layer at the boundary likewise drops. Increasing values of Nb have an impact on the Brownian motion, which also restricts the nanoparticle diffusion in the flow regime and reduces the concentration of the fluid. Thus, an increase in Nb reduces  $\phi(\eta)$ . At the sheet surface, the concentration of the nanofluid shows dominant behavior compared to the hybrid nanofluid. However, this effect is reversed above the surface. Figures 12 and 13 show the impression of thermal Biot number (Bi) on  $\theta(n)$  and  $\phi(n)$ . Both  $\theta(n)$  and  $\phi(n)$  augment with increasing values of Bi. The reason is that increasing Bi augments the thermal flow, which results in intensification in the heat transfer rate. The increase in the thermal flow rate leads to the enhancement of the thickness of the thermal boundary layer. Thus,  $\theta(\eta)$  increases with increasing Bi. Similarly. Bi also augments the concentration boundary layer thickness and thus  $\phi(\eta)$  increases. At the sheet surface, the concentration of the nanofluid shows a dominant behavior compared to the hybrid nanofluid. However, this effect is reversed above the surface. Figure 14 shows the influence of E on  $\phi(\eta)$ . It was found that an increase in E augments  $\phi$ ( $\eta$ ). It was observed that at lower temperatures and higher E, the reaction rate decreases, thereby slowing the chemical process; as a result, the thickness of the concentration boundary layer increases, which increases  $\phi(\eta)$ . Furthermore, the impact of E is higher for the hybrid nanofluid compared to the nanofluid flow. Figure 15 shows the influence of the reaction factor  $(K_r)$  on  $\phi(\eta)$ . It was found that an increase in  $K_r$  reduces  $\phi(\eta)$ . Actually, the increase in the  $(1 + \omega\theta)$ ). Thus, increasing chemical reaction takes place and reduces the thickness of the concentration boundary layer,

**Table 7:** Impacts of  $\chi_2$ , Bi, and  $\theta_w$  on  $\frac{1}{\sqrt{Re_r}}$  Nu

<b>χ</b> <sub>2</sub>	Ві	$\theta_{\sf w}$	Ag−H₂O nanofluid
0.01	0.1	1.1	0.470863
0.02			0.480849
0.03			0.495185
0.04			0.515890
	0.3		0.415759
	0.7		0.479058
	1.3		0.568561
		1.1	0.487657
		1.2	0.496426
		1.3	0.509264

which results in the reduction of the concentration distribution. Thus, an increase in  $K_r$  reduces  $\phi(\eta)$ . Furthermore, the concentration of the nanofluid flow is lower than the flow of the hybrid nanoliquid. Figure 16 demonstrates the impact of Sc on  $\phi(\eta)$ . An increase in Sc reduces the diffusion of mass. Therefore, an increase in Sc diminishes  $\phi(\eta)$ . Moreover, the concentration of the hybrid nanoparticles flow is greater than the flow of the nanofluid. Table 3 shows the influences of  $\chi_1$  and M on  $\sqrt{\text{Re}_r} C_f$ . The increasing  $\chi_1$  and M augment  $\sqrt{\text{Re}_{r}}C_{f}$ . The reason is that the higher volume fraction of the solid nanoparticles increases the shear stress, which consequently increases the skin friction at the surface. Thus,  $\sqrt{\text{Re}_{\text{r}}} C_{\text{f}}$  increases with an increase in  $\chi_1$ . Also, an increase in M increases  $\sqrt{\text{Re}_{r}}C_{f}$ . An increase in M generates Lorentz force, which results in higher friction force at the surface. Thus, an increase in M reduces  $\sqrt{\text{Re}_r} C_f$ . The same findings can be found in Tables 4 and 5. From these tables, it can be found that the friction force for the hybrid nanofluid was found to be the highest. Table 6 shows the impacts of  $\chi_1$ , Bi, and  $\theta_{\rm w}$  on  $\frac{1}{\sqrt{\rm Re}}$  Nu. An increase in  $\chi_1$ , Bi and  $\theta_{\rm w}$  augments  $\frac{1}{\sqrt{\text{Re}_r}}$ Nu. Thus,  $\frac{1}{\sqrt{\text{Re}_r}}$ Nu increases with increasing  $\chi_1$ . Similarly, an increase in Bi enhances the coefficient of heat transmission, which consequently augments the rate of thermal flow of the nanofluid. Hence, the higher Bi heightens  $rac{1}{\sqrt{Re_r}}$ Nu. The same impact of  $heta_w$  is found for  $rac{1}{\sqrt{Re_r}}$ Nu. The same findings can be found in Tables 7 and 8. As shown in the tables, the heat transmission rate for the hybrid nanofluid was found to be the highest. The Ag-H<sub>2</sub>O nanofluid has a 3% greater impact on  $\sqrt{\text{Re}_r} C_f$  than the CuO-H<sub>2</sub>O nanofluid. Similarly, the CuO-Ag/H2O hybrid nanofluid has a 28% higher impact on  $\sqrt{\text{Re}_r}C_f$  than the Ag-H<sub>2</sub>O nanofluid. Also, the CuO-Ag/H<sub>2</sub>O hybrid nanofluid has a 26% higher impact on  $\sqrt{\mathrm{Re_r}}\,C_\mathrm{f}$  than the CuO–H $_2$ O nanofluid. The heat transfer rate

**Table 8:** Impacts of  $\chi_1 = \chi_2$ , Bi, and  $\theta_w$  on  $\frac{1}{\sqrt{Re_r}}$  Nu

$\chi_1 = \chi_2$	Bi	$\boldsymbol{\theta}_{w}$	CuO−Ag/H₂O hybrid nanofluid
0.01	0.1	1.1	0.588648
0.02			0.607529
0.03			0.598620
0.04			0.637863
	0.3		0.654264
	0.7		0.670834
	1.3		0.696431
		1.1	0.523574
		1.2	0.547627
		1.3	0.568973

of the Ag-H<sub>2</sub>O nanofluid is 3% greater than the CuO-H<sub>2</sub>O

nanofluid. Also, the heat transfer rate of the CuO-Ag/H<sub>2</sub>O hybrid nanofluid is 28% higher than the Ag-H<sub>2</sub>O nanofluid.

### 6 Conclusion

This section presents the concluding remarks that are observed from the present analysis. The current study is done for a time-independent water-based hybrid nanofluid flow over a rotating disk surface. In this investigation, two different nanoparticles, namely copper oxide and silver, are chosen. In the present analysis, the flow is considered to be Newtonian. The influence of the magnetic field, thermophoresis, nonlinear thermal radiation, chemical reaction, Brownian motion, and activation energy is taken into account. A numerical solution using the bvp4c technique is accomplished using MATLAB software. The present results are compared with the previous literature and it is found to have a close relationship with previous studies. From this investigation, the following concluding points are found:

- a) A higher magnetic parameter causes the surface to experience more friction, which lowers the radial and azimuthal velocity profiles. When compared to the nanofluid, the hybrid nanofluid's radial velocity at the sheet surface exhibits dominant behavior.
- b) The thermal and concentration profiles are enhanced by the higher thermal radiation factor. In comparison to the nanofluid, the temperature and concentration of the nanofluid exhibit dominant behavior near the sheet surface. Above the surface, though, this impact is the opposite.
- c) The temperature profiles are enhanced when thermophoresis, temperature ratio, and heat source parameters increase. When compared to a hybrid nanofluid, the temperature of the nanofluid exhibits dominant behavior near the sheet surface. Above the surface, though, this impact is the opposite.
- d) The concentration profile is enhanced by the thermophoresis factor and decreased by the Brownian motion factor. When compared to a hybrid nanofluid, the concentration profiles of the former exhibit dominant behavior at the sheet surface. Above the surface, though, this impact is the opposite.
- e) The Biot number increases with the concentration and temperature profiles. Additionally, in comparison to the hybrid nanofluid, the concentration of the nanofluid exhibits dominant behavior near the sheet surface. Above the surface, though, this impact is the opposite.

- f) The skin friction at the disk's surface is increased by the increase in the solid volume fraction and magnetic component. Moreover, the hybrid nanofluid flow is observed to have a greater surface drag.
- g) The rate of heat transmission is accelerated by a greater solid volume fraction, temperature ratio, and Biot number. Furthermore, a greater rate of heat transfer is observed in the case of the hybrid nanofluid flow.

### 7 Future recommendations

In the future, the present mathematical model can be extended to study ternary hybrid nanofluid flow over a rotating disk surface by including three different metallic and nonmetallic nanoparticles. Furthermore, the addition of the Cattaneo-Christov heat and mass flux model can be studied to analyze heat and mass transport phenomena.

**Acknowledgments:** This study was supported by the Princess Nourah bint Abdulrahman University Researchers Supporting Project number (PNURSP2024R443), Princess Nourah bint Abdulrahman University, Riyadh, Saudi Arabia. This work was also supported by the Deanship of Scientific Research, the Vice Presidency for Graduate Studies and Scientific Research, King Faisal University, Saudi Arabia (KFU241370).

**Funding information:** This study was supported by the Princess Nourah bint Abdulrahman University Researchers Supporting Project number (PNURSP2024R443), Princess Nourah bint Abdulrahman University, Riyadh, Saudi Arabia. This work was supported by the Deanship of Scientific Research, the Vice Presidency for Graduate Studies and Scientific Research, King Faisal University, Saudi Arabia (KFU241370).

Author contributions: Humaira Yasmin: conceptualization, methodology, software, funding, reviewing, and editing. Laila A. AL-Essa: data curation, writing – reviewing, and editing. Ali M. Mahnashi: visualization and investigation. Waleed Hamali: software, validation, and supervision. Anwar Saeed: writing – original draft preparation. All authors have accepted responsibility for the entire content of this manuscript and approved its submission.

**Conflict of interest:** The authors state no conflict of interest.

**Data availability statement:** All data generated or analyzed during this study are included in this published article.

### References

- Choi, S. U. S. and J. A. Eastman. Enhancing thermal conductivity of fluids with nanoparticles. 1995 International mechanical engineering congress and exhibition, San Francisco, CA, United States, Nov 1995.
- Shahzad, F., W. Jamshed, S. M. El Din, M. Shamshuddin, R. W. Ibrahim, and Z. Raizah. Second-order convergence analysis for Hall effect and electromagnetic force on ternary nanofluid flowing via rotating disk. Scientific Reports, Vol. 12, 2022, pp. 1-21.
- Shamshuddin, M. D., N. Akkurt, A. Saeed, and P. Kumam. Radiation mechanism on dissipative ternary hybrid nanoliquid flow through rotating disk encountered by Hall currents: HAM solution. Alexandria Engineering Journal, 2022.
- Pasha, A. A., N. Islam, W. Jamshed, M. I. Alam, A. G. A. Jameel, K. A. Juhany, et al. Statistical analysis of viscous hybridized nanofluid flowing via Galerkin finite element technique. The International Communications in Heat and Mass Transfer, Vol. 137, 2022, id. 106244.
- Shah, Z., A. Khan, W. Khan, M. K. Alam, S. Islam, P. Kumam, et al. Micropolar gold blood nanofluid flow and radiative heat transfer between permeable channels. Computer Methods and Programs in Biomedicine, Vol. 186, 2020, id. 105197.
- Asghar, A. and T. Y. Ying. Zaimi WMKAW. Two-dimensional mixed convection and radiative Al2O3-Cu/H2O hybrid nanofluid flow over a vertical exponentially shrinking sheet with partial slip conditions. CFD Letter, Vol. 14, 2022, pp. 22-38.
- Khan, A., W. Kumam, I. Khan, A. Saeed, T. Gul, P. Kumam, et al. [7] Chemically reactive nanofluid flow past a thin moving needle with viscous dissipation, magnetic effects and hall current. PLoS One, Vol. 16, 2021, id. e0249264.
- Haider, J. A., S. Ahmad, H. A. Ghazwani, M. Hussien, M. Y. Almusawa, and E. A. Az-Zo'bi. Results validation by using finite volume method for the blood flow with magnetohydrodynamics and hybrid nanofluids. Modern Physics Letters B, 2024, id. 2450208.
- Akhtar, S., Z. Hussain, H. A. Ghazwani, S. A. Lone, and E. A. Az-Zo'bi. Computational fluid dynamics analysis on endoscopy of main left coronary artery: An application of applied mathematics. Heliyon, 2024.
- [10] Naveed Khan, M., A. A. Khan, M., A. Algahtani, Z. Wang, H. A. Hejazi, and E. A. Az-Zo'bi. Chemically reactive aspects of stagnation-point boundary layer flow of second-grade nanofluid over an exponentially stretching surface. Numerical Heat Transfer, Part B: Fundamentals, 2024, pp. 1-17.
- [11] Ahsan, N., M. N. Aslam, M. N. Khan, and E. A. Az-Zo'bi. Bioconvective flow analysis of non-newtonian fluid over a porous curved stretching surface. Proceedings of the Institution of Mechanical Engineers, Part N: Journal of Nanomaterials, Nanoengineering and Nanosystems, 2024, 23977914241231892.
- Kanwal, S., S. A. A. Shah, A. Bariq, B. Ali, A. E. Ragab, and E. A. Az-Zo'bi. Insight into the dynamics of heat and mass transfer in nanofluid flow with linear/nonlinear mixed convection, thermal radiation, and activation energy effects over the rotating disk. Scientific Reports, Vol. 13, 2023, id. 23031.
- Waseem, M., T. Gul, I. Khan, A. Khan, A. Saeed, I. Ali, et al. Gravitydriven hydromagnetic flow of couple stress hybrid nanofluid with homogenous-heterogeneous reactions. Scientific Reports, Vol. 11, 2021, pp. 1-12.
- [14] Hussain, M. A., F. Jamil, A. Ejaz, A. Wakeel, S. Khalid, H. M. Ali, et al. Thermal performance of sintered copper wick heat pipe using water-based hybrid nanofluids: an experimental study. Journal of Porous Materials, 2022, id. 25.

- [15] Guedri, K., A. Khan, N. Sene, Z. Raizah, A. Saeed, and A. M. Galal. Thermal Flow for radiative ternary hybrid nanofluid over nonlinear stretching sheet subject to Darcy-Forchheimer phenomenon. Mathematical Problems in Engineering, 2022, id. 2022.
- [16] Zhang, L., M. M. Bhatti, E. E. Michaelides, M. Marin, and R. Ellahi. Hybrid nanofluid flow towards an elastic surface with tantalum and nickel nanoparticles, under the influence of an induced magnetic field. European Physical Journal: Special Topics, Vol. 231, 2022, pp. 521-33.
- Ojjela, O. Numerical investigation of heat transport in [17] Alumina-Silica hybrid nanofluid flow with modeling and simulation. Mathematics and Computers in Simulation, Vol. 193, 2022,
- [18] Gumber, P., M. Yaseen, S. K. Rawat, and M. Kumar. Heat transfer in micropolar hybrid nanofluid flow past a vertical plate in the presence of thermal radiation and suction/injection effects. Partial Differential Equations in Applied Mathematics, Vol. 5, 2022, id. 100240.
- [19] Sriharan, G., S. Harikrishnan, and H. M. Ali. Enhanced heat transfer characteristics of the mini hexagonal tube heat sink using hybrid nanofluids. Nanotechnology, Vol. 33, 2022, id. 475403.
- Ullah, H., M. Shoaib, R. A. Khan, K. S. Nisar, M. A. Z. Raja, and S. [20] Islam. Soft computing paradigm for heat and mass transfer characteristics of nanofluid in magnetohydrodynamic (MHD) boundary layer over a vertical cone under the convective boundary condition. International journal of simulation modelling, 2023, pp. 1-25.
- [21] Zawawi, N. N. M., W. H. Azmi, M. F. Ghazali, and H. M. Ali. Performance of air-conditioning system with different nanoparticle composition ratio of hybrid nanolubricant. Micromachines, Vol. 13, 2022, id. 1871.
- [22] Asghar, A., L. A. Lund, Z. Shah, N. Vrinceanu, W. Deebani, and M. Shutaywi. Effect of thermal radiation on three-dimensional magnetized rotating flow of a hybrid nanofluid. Nanomaterials, Vol. 12,
- [23] Babar, H., H. Wu, H. M. Ali, T. R. Shah, and W. Zhang. Staggered oriented airfoil shaped pin-fin heat sink: Investigating the efficacy of novel water based ferric oxide-silica hybrid nanofluid. International Journal of Heat and Mass Transfer, Vol. 194, 2022, id. 123085.
- [24] Akbar, A., H. Ullah, M. A. Z. Raja, K. S. Nisar, S. Islam, and M. Shoaib. A design of neural networks to study MHD and heat transfer in two phase model of nano-fluid flow in the presence of thermal radiation. Waves in Random and Complex Media, 2022, pp. 1-24.
- [25] Ullah, H., S. Islam, and M. Fiza. Analytical solution for threedimensional problem of condensation film on inclined rotating disk by extended optimal homotopy asymptotic method. The Iranian Journal of Science and Technology, Transactions of Mechanical Engineering, Vol. 40, 2016, pp. 265-73.
- [26] Raja, M. A. Z., K. S. Nisar, M. Shoaib, A. Akbar, H. Ullah, and S. Islam. A predictive neuro-computing approach for micro-polar nanofluid flow along rotating disk in the presence of magnetic field and partial slip. AIMS Mathematics, Vol. 8, 2023, pp. 12062-92.
- Ullah, H., K. Ullah, M. A. Z. Raja, M. Shoaib, K. S. Nisar, S. Islam, et al. Numerical treatment of squeezed MHD Jeffrey fluid flow with Cattaneo Chrisstov heat flux in a rotating frame using Levnberg-Marquard method. Alexandria Engineering Journal, Vol. 66, 2023,
- [28] Vishalakshi, A. B., U. S. Mahabaleshwar, and I. E. Sarris. An MHD fluid flow over a porous stretching/shrinking sheet with slips and mass transpiration. Micromachines, Vol. 13, 2022, id. 116.

- [29] Asjad, M. I., M. Zahid, M. Inc, D. Baleanu, and B. Almohsen. Impact of activation energy and MHD on Williamson fluid flow in the presence of bioconvection. *Alexandria Engineering Journal*, Vol. 61, 2022, pp. 8715–27.
- [30] Bejawada, S. G., Y. D. Reddy, W. Jamshed, K. S. Nisar, A. N. Alharbi, and R. Chouikh. Radiation effect on MHD Casson fluid flow over an inclined non-linear surface with chemical reaction in a Forchheimer porous medium. *Alexandria Engineering Journal*, Vol. 61, 2022, pp. 8207–20.
- [31] Usman, M., T. Gul, A. Khan, A. Alsubie, and M. Z. Ullah. Electromagnetic couple stress film flow of hybrid nanofluid over an unsteady rotating disc. *The International Communications in Heat* and Mass Transfer, Vol. 127, 2021, id. 105562.
- [32] Sharma, K., S. Kumar, A. Narwal, F. Mebarek-Oudina, and I. L. Animasaun. Convective MHD fluid flow over stretchable rotating disks with dufour and Soret effects. *International Journal of Applied and Computational Mathematics*, Vol. 8, 2022, pp. 1–12.
- [33] Asghar, A., N. Vrinceanu, T. Y. Ying, L. A. Lund, Z. Shah, and V. Tirth. Dual solutions of convective rotating flow of three-dimensional hybrid nanofluid across the linear stretching/shrinking sheet. *Alexandria Engineering Journal*, Vol. 75, 2023, pp. 297–312.
- [34] Rasool, G., W. Xinhua, L. A. Lund, U. Yashkun, A. Wakif, and A. Asghar. Dual solutions of unsteady flow of copper-alumina/water based hybrid nanofluid with acute magnetic force and slip condition. *Heliyon*, Vol. 9, 2023.
- [35] Lund, L. A., A. Asghar, G. Rasool, and U. Yashkun. Magnetized casson SA-hybrid nanofluid flow over a permeable moving surface with thermal radiation and Joule heating effect. Case Stud. *Thermal Engineering*, Vol. 50, 2023, id. 103510.
- [36] Tarakaramu, N., P. V. Satya Narayana, R. Sivajothi, K. Bhagya Lakshmi, D. Harish Babu, and B. Venkateswarlu. Three-dimensional non-Newtonian couple stress fluid flow over a permeable stretching surface with nonlinear thermal radiation and heat source effects. *Heat Transfer*, Vol. 51, 2022, pp. 5348–67.
- [37] Nasir, S., S. Sirisubtawee, P. Juntharee, A. S. Berrouk, S. Mukhtar, and T. Gul. Heat transport study of ternary hybrid nanofluid flow under magnetic dipole together with nonlinear thermal radiation. *Applied Nanoscience*, Vol. 12, 2022, pp. 2777–88.
- [38] Shaw, S., S. S. Samantaray, A. Misra, M. K. Nayak, and O. D. Makinde. Hydromagnetic flow and thermal interpretations of Cross hybrid nanofluid influenced by linear, nonlinear and quadratic thermal radiations for any Prandtl number. *The International Communications in Heat and Mass Transfer*, Vol. 130, 2022, id. 105816.
- [39] Owhaib, W. and W. Al-Kouz. Three-dimensional numerical analysis of flow and heat transfer of bi-directional stretched nanofluid film exposed to an exponential heat generation using modified Buongiorno model. *Science Reports*, Vol. 12, 2022, pp. 1–20.
- [40] Waqas, H., M. Oreijah, K. Guedri, S. U. Khan, S. Yang, S. Yasmin, et al. Gyrotactic motile microorganisms impact on pseudoplastic nanofluid flow over a moving Riga surface with exponential heat flux. *Crystals*, Vol. 12, 2022, id. 1308.
- [41] Samrat, S. P., Y. H. Gangadharaiah, G. P. Ashwinkumar, and N. Sandeep. Effect of exponential heat source on parabolic flow of three different non-Newtonian fluids. *Proceedings of the Institution of Mechanical Engineers, Part E: Journal of Process Mechanical Engineering*, 2022, id. 09544089221083468.
- [42] Qian, W.-M., M. I. Khan, F. Shah, M. Khan, Y.-M. Chu, W. A. Khan, et al. Mathematical modeling and MHD flow of micropolar fluid toward an exponential curved surface: heat analysis via ohmic

- heating and heat source/sink. *Arabian Journal for Science and Engineering*, Vol. 47, 2022, pp. 867–78.
- [43] Ramzan, M., J. Ali, N. Shahmir, H. A. S. Ghazwani, K. S. Nisar, and C. A. Saleel. Thermophoretic particle deposition impact in the Oldroyd-B fluid flow influenced by a magnetic dipole with an exponential thermal heat source. *International Journal of Modern Physics B: Condensed Matter Physics, Statistical Physics, Applied Physics*, 2022, id. 2350059.
- [44] Haq, S. U., S. U. Jan, R. Bilal, J. H. Alzahrani, I. Khan, and A. Alzahrani. Heat-mass transfer of MHD second grade fluid flow with exponential heating, chemical reaction and porosity by using fractional Caputo-Fabrizio derivatives. Case Studies in Thermal Engineering, Vol. 36, 2022. id. 102104
- [45] Alqarni, M. M., M. Bilal, R. Allogmany, E. Tag-Eldin, M. E. Ghoneim, and M. F. Yassen. Mathematical analysis of Casson fluid flow with energy and mass transfer under the influence of activation energy from a non-coaxially spinning disc. Frontiers in Energy Research, 2022, id. 10.
- [46] Rekha, M. B., I. E. Sarris, J. K. Madhukesh, K. R. Raghunatha, and B. C. Prasannakumara. Activation energy impact on flow of AA7072-AA7075/Water-Based hybrid nanofluid through a cone, wedge and plate. *Micromachines*, Vol. 13, 2022, id. 302.
- [47] Abbasi, A., S. U. Khan, K. Al-Khaled, M. I. Khan, W. Farooq, A. M. Galal, et al. Thermal prospective of Casson nano-materials in radiative binary reactive flow near oblique stagnation point flow with activation energy applications. *Chemical Physics Letters*, Vol. 786, 2022, id. 139172.
- [48] Ayub, A., T. Sajid, W. Jamshed, W. R. M. Zamora, L. A. V. More, L. M. G. Talledo, et al. Activation energy and inclination magnetic dipole influences on Carreau nanofluid flowing via cylindrical channel with an infinite shearing rate. *Applied Science*, Vol. 12, 2022, id. 8779.
- [49] Khan, U., S. Bilal, A. Zaib, O. D. Makinde, and A. Wakif. Numerical simulation of a nonlinear coupled differential system describing a convective flow of Casson gold–blood nanofluid through a stretched rotating rigid disk in the presence of Lorentz forces and nonlinear thermal radiation. *Numerical Methods for Partial Differential Equations*, 2020.
- [50] Turkyilmazoglu, M. MHD fluid flow and heat transfer due to a stretching rotating disk. *International Journal of Thermal Sciences*, Vol. 51, 2012, pp. 195–201.
- [51] Mustafa, I., T. Javed, and A. Ghaffari. Heat transfer in MHD stagnation point flow of a ferrofluid over a stretchable rotating disk. *Journal of Molecular Liquids*, Vol. 219, 2016, pp. 526–32.
- [52] Dawar, A., S. Islam, Z. Shah, and S. R. Mahmuod. A passive control of casson hybrid nanofluid flow over a curved surface with alumina and copper nanomaterials: a study on sodium alginate-based fluid. *Journal of Molecular Liquids*, 2023, id. 122018.
- [53] Dawar, A., A. Wakif, T. Thumma, and N. A. Shah. Towards a new MHD non-homogeneous convective nanofluid flow model for simulating a rotating inclined thin layer of sodium alginate-based Iron oxide exposed to incident solar energy. *The International Communications in Heat and Mass Transfer*, Vol. 130, 2022, id. 105800.
- [54] Shafiq, A., G. Rasool, H. Alotaibi, H. M. Aljohani, A. Wakif, I. Khan, et al. Thermally enhanced Darcy-Forchheimer Casson-water/gly-cerine rotating nanofluid flow with uniform magnetic field. *Micromachines*, Vol. 12, 2021, id. 605.
- [55] Alghamdi, M., A. Wakif, T. Thumma, U. Khan, D. Baleanu, and G. Rasool. Significance of variability in magnetic field strength and heat source on the radiative-convective motion of sodium alginate-

- based nanofluid within a Darcy-Brinkman porous structure bounded vertically by an irregular slender surface. *Case Studies in Thermal Engineering*, Vol. 28, 2021, id. 101428.
- [56] Von Kármán, T. Uber laminare und turbulente Reibung. Zeitschrift fuer Angewandte Mathematik und Mechanik, Vol. 1, 1921, pp. 233–52.
- [57] Ragupathi, P., T. Muhammad, S. Islam, and A. Wakif. Application of Arrhenius kinetics on MHD radiative Von Kármán Casson nanofluid flow occurring in a Darcy-Forchheimer porous medium in the presence of an adjustable heat source. *Physica Scripta*, Vol. 96, 2021, id. 125228.
- [58] Shampine, L. F., J. Kierzenka, and M. W. Reichelt. Solving boundary value problems for ordinary differential equations in MATLAB with bvp4c. *Tutorial Notes*, Vol. 2000, 2000, pp. 1–27.

- [59] Dharmaiah, G., S. Dinarvand, P. Durgaprasad, and S. Noeiaghdam. Arrhenius activation energy of tangent hyperbolic nanofluid over a cone with radiation absorption. *Results Engineering*, Vol. 16, 2022, id. 100745.
- [60] Xia, W.-F., S. Ahmad, M. N. Khan, H. Ahmad, A. Rehman, J. Baili, et al. Heat and mass transfer analysis of nonlinear mixed convective hybrid nanofluid flow with multiple slip boundary conditions. Case Studies in Thermal Engineering, Vol. 32, 2022, id. 101893.
- [61] Rashidi, M. M., S. Abelman, and N. F. Mehr. Entropy generation in steady MHD flow due to a rotating porous disk in a nanofluid. *International Journal of Heat and Mass Transfer*, Vol. 62, 2013, pp. 515–25.
- [62] Turkyilmazoglu, M. Purely analytic solutions of magnetohydrodynamic swirling boundary layer flow over a porous rotating disk. *Computers and Fluids*, Vol. 39, 2010, pp. 793–9.